encit 2020

ABCM Associação Brasileira de Engenharia e Ciências Mecânicas

18th Brazilian Congress of Thermal Sciences and Engineering
November 16–20, 2020 (Online)

ENC-2020-0807
DETAILED NUMERICAL SIMULATION OF THE FLAME-FLOW INTERACTION IN A SLOT-BURNER LAMINAR PREMIXED FLAME

Rafael Becker Meier
Amir Antônio Martins Oliveira
Universidade Federal de Santa Catarina
rafael.meier@labcet.ufsc.br
amir.oliveira@gmail.com

Abstract. *The purpose of this work is to numerically simulate the premixed flame stabilized in a slot burner with the aim of capturing transport effects that change the local flame stretch and consumption speed. Stoichiometric and lean flames of methane and dimethyl-ether with air at atmospheric pressure are simulated using a two-dimensional cartesian formulation for the low-Mach number compressible flow, with heat transfer and detailed mass transport effects. Reduced mechanisms with 17 species and 58 elementary reactions and 30 species and 175 reactions, with 9 species treated under quasi-steady state, were used for methane and dimethyl-ether respectively. The thermodynamics and kinetics are solved in Cantera library while the transport equations are solved using the OpenFOAM. The flame sheet curvature, strain and stretch rates are locally calculated using two different definitions for the location of the flame sheet. The results evidence the effects of the definition of the flame sheet location in the flame kinematics. The behaviors of the Karlovitz number and displacement speed in the positive and negative curvature regions are observed and all flames exhibit approximately the same general correlation between the flame displacement speed normalized by the laminar flame speed (planar flame) and Karlovitz number. The mass fraction of hydrogen along the flame surface presents strong deficiency in the positive curvature region and strong excess in the negative curvature region when compared to the planar, adiabatic flame. The trend is observed not only on the position of the flame surface, but also in the entire distribution along the normal direction as well.*

Keywords: *premixed combustion, laminar premixed flame, flame aerodynamics, DNS*

1. INTRODUCTION

The increase in energy efficiency and fuel flexibility requirements for internal combustion engines and gas turbines have pushed the development of premixed and partially premixed mixture combustion systems to work under higher pressure, higher temperature and leaner mixtures.

Premixed flames are characterized by their apparent and consumption flame speed (Poinsot and Veynante, 2005). The consumption flame speed results from the temperature and species distribution within the flame, while the apparent flame speed is a consequence of the interaction with the unburned flow field. Under a flame sheet approximation, the preheating and reaction zones are collapsed into an infinitesimally thin region. In respect to this flame surface, the unburned flow field may have normal and tangential components. The normal component advects the flame sheet, developing flame curvature that interacts with thermal-diffusive and flow instabilities. The tangent component causes flame stretch, which is also present in a transient flame.

When subjected to a higher magnification, the laminar flame presents outer and inner structures: a preheating zone, with thickness δ_l, characterized by temperature and species mass fraction gradients, and a reaction zone, with thickness $\delta_r \ll \delta_l$, characterized by a distributed reaction region. The flame curvature changes the gradients of temperature and chemical species concentration in the preheating zone, changing the direction of the heat and mass transport vectors. These in turn affect the flame structure by changing the temperature and species concentrations in the reaction zone. The flame then seeks a new equilibrium structure and position in respect to the flow field. This interplay has important effects in many combustion phenomena such as flame stabilization, flashback, blowout, and local extinction and re-ignition (Law, 2006).

When flame sheet theories are compared to flame structure simulations, several aspects are undefined a priori, e.g., which isotherm or isoconcentration surface defines the position of the flame front, on which the flame curvature and stretch are calculated. Therefore, describing a complete laminar flame structure in terms of flame kinematics parameters is not a direct exercise.

Here, the interplay between flow and flame position and structure is analyzed in a slot-burner flame. This flame is two-

dimensional, allowing for faster computation, as well as, easier tracking and visualization. It has been modeled elsewhere, e.g., Selle *et al.* (2011), allowing for comparison of alternative strategies. The focus here are: (1) developing and testing algorithms for premixed flame simulation and tracking, (2) analyzing the flame kinematics under different definitions of the location of the flame sheet, and (3) analyzing the effect of flame curvature in local stretch rate, displacement speed, transport and reaction within the flame.

2. THEORETICAL BACKGROUND

The following approach is discussed in Peters (2000), Poinsot and Veynante (2005), and Law (2006). The original works are acknowledged in those references.

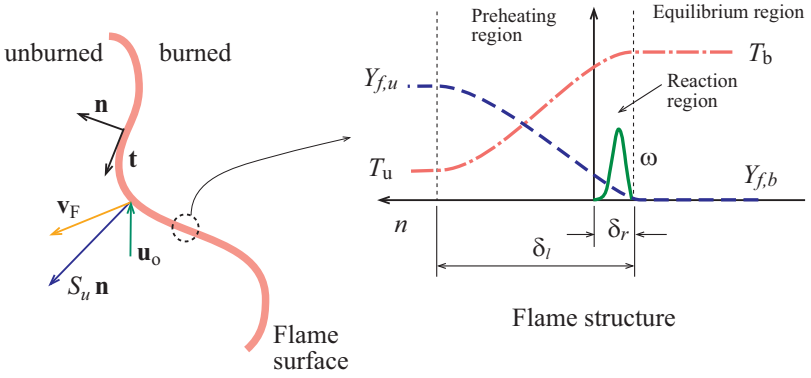

Figure 1: Flame sheet approximation and laminar flame structure.

The flame speed is defined as the propagation speed of a deflagration wave relative to the unburned mixture velocity. It has a precise meaning when the flame is planar and propagates steadily because the mass flow rate through the flame is constant and uniform. In this reference flame, the entire structure travels consuming the unburned mixture at a constant speed S_l^0. For multidimensional flows, the flame speed is a local property because the mass flow rate through the flame is neither constant, nor uniform. In multidimensional flow, the flame undergoes a continuous stretching, which affects the transport rates and results in a change of the flame speed. Figure 1 presents the flame surface separating the burned and unburned mixture, a flame sheet approximation, and the laminar flame structure, which will be basis for a thin flame approximation. The objective of the following sections is to estimate the flame speed of stretched flames.

2.1 Flame sheet approximation

A phenomenological relation between flame speed and flame stretch can be obtained in the framework of a hydrodynamic model based on a flame sheet approximation (Matalon *et al.*, 2003). Assuming that the flame is a surface of discontinuity separating the unburned from the burned mixtures, the flame stretch rate, K, is defined as the fractional rate of change of a Lagrangian flame surface element A,

$$\mathrm{K} = \frac{1}{A}\frac{dA}{dt}. \tag{1}$$

The stretch rate is positive when the flame surface expands and negative otherwise. Assuming that the local flame speed S_l is affected by the stretch rate, a perturbation of the laminar (planar) flame speed $S_l(0) = S_l^0$ by the local stretch rate $(\mathrm{K} - 0)$ can be represented as

$$S_l(\mathrm{K}) = S_l(0) + \frac{\partial S_l(0)}{\partial \mathrm{K}}(\mathrm{K}-0) + \frac{1}{2!}\frac{\partial^2 S_l(0)}{\partial \mathrm{K}^2}(\mathrm{K}-0)^2 + \ldots + \frac{1}{n!}\frac{\partial^n S_l(0)}{\partial \mathrm{K}^n}(\mathrm{K}-0)^n. \tag{2}$$

The first-order sensitivity coefficient of the flame speed to stretch rate is referred to as the Markstein length,

$$\mathscr{L} = -\frac{\partial S_l(0)}{\partial \mathrm{K}}. \tag{3}$$

For weakly-stretched flames, the linear regime for the stretched flame may be represented as

$$S_l = S_l^0 - \mathscr{L}\mathrm{K}. \tag{4}$$

In this linear regime, the Markstein length $\mathscr{L}$ becomes a phenomenological parameter that depends on the properties of the unburned mixture.

The flame stretch rate is simply associated to the flame curvature and flow velocity as,

$$\mathrm{K} = S_l^o \ (\nabla \cdot \vec{n}) - \vec{n} \cdot \nabla \vec{u}_o \cdot \vec{n}. \tag{5}$$

In this model, the displacement velocity of the flame surface is associated to S_l^o. The first term in the right-hand side is the effect of flame curvature $\kappa = \nabla \cdot \vec{n}$. The second term is the strain rate imposed on the flame by flow velocity gradients.

Using δ_l^0 and S_l^0 as characteristic length and velocity scales, the nondimensional form of Eq. (4) becomes

$$\frac{S_l}{S_l^0} = 1 - \mathrm{Ma}\,\mathrm{Ka}, \tag{6}$$

where $\mathrm{Ka} = \mathrm{K}(\delta_l^0/S_l^0)$ is the nondimensional stretch rate, or Karlovitz number, and $\mathrm{Ma} = \mathscr{L}/\delta_l^0$ is the Markstein number. The Karlovitz number is a ratio of the flame characteristic time scale $t_l \sim \delta_l^0/S_l^0$ and the stretch characteristic time scale $t_\mathrm{K} \sim 1/\mathrm{K}$, i.e., the time required to double the flame surface area. From the laminar flame characteristic length and speed scales,

$$\delta_l^0 \sim \frac{D_T}{S_l^0}, \quad \left(S_l^0\right)^2 \sim \frac{D_T}{\rho_u}\dot{\omega}_f, \tag{7}$$

where D_T is the thermal diffusivity and $\dot{\omega}_f$ is an overall fuel reaction rate, the Karlovitz number becomes

$$\mathrm{Ka} = \mathrm{K}\frac{\delta_l^0}{S_l^0} \sim \frac{\rho_u \mathrm{K}}{\dot{\omega}_f}. \tag{8}$$

This relation expresses that the effects of curvature are more pronounced for weakly burning flames, such as in lean and near extinction conditions.

The Markstein number represents the sensitivity of the flame speed to flame stretch. Fuel rich hydrogen and fuel lean hydrocarbon flames present fuel Lewis number $\mathrm{Le} > 1$ and $\mathscr{L} > 0$. Fuel lean hydrogen and fuel rich hydrocarbon flames present fuel Lewis number $\mathrm{Le} < 1$ and $\mathscr{L} < 0$.

The Eqs. (4) and (5) are used in the G-equation model for the flame surface approximation (Peters, 2000). This is the essence of the hydrodynamic model. This model lacks in the approximation for the displacement velocity and a more precise definition of flame stretch rate. These are addressed next.

3. Flame stretch rate

The flame stretch rate can be directly related to the kinematics of the flame surface. The flame displacement velocity is defined as the normal component of the relative velocity of the flame surface in respect to the flow. It differs from the laminar (planar) flame speed because of flame curvature and unsteadiness. Naming S_d the displacement speed and $\vec{u}_o$ the flow velocity of the unburned mixture in the vicinity of the flame surface, the local propagation velocity of the flame surface $\vec{v}_F$ is

$$\vec{v}_F = \vec{u}_o + \ S_d \vec{n}, \tag{9}$$

where $S_d\ \vec{n}$ is the displacement velocity and $\vec{n}$ is the normal unit vector at the flame surface, pointed to the unburned mixture side.

Starting from Eq. (1), the flame stretch rate may be expressed in different equivalent forms (Law, 2006):

$$\begin{aligned} \mathrm{K} &= \nabla_t \cdot \vec{v}_{F,t} + (\vec{v}_F \cdot \vec{n})\,(\nabla \cdot \vec{n}), \\ &= \nabla_t \cdot \vec{u}_{o,t} + S_F\,(\nabla \cdot \vec{n}), \\ &= \nabla \cdot \vec{n} \times (\vec{u}_o \times \vec{n}) + (\vec{u}_o \cdot \vec{n})\,(\nabla \cdot \vec{n}) + S_d\,(\nabla \cdot \vec{n}). \end{aligned} \tag{10}$$

In these equations, ∇_t is the nabla operator along a plane tangent to the flame surface. The first term in the right-hand side, $\nabla_t \cdot \vec{v}_F = \nabla_t \cdot \vec{v}_{F,t} = \nabla_t \cdot \vec{u}_{o,t} = \nabla \cdot \vec{n} \times (\vec{u}_o \times \vec{n}) = -\vec{n} \cdot \nabla \times (\vec{u}_o \times \vec{n})$, is the tangential strain rate related to the flow-nonuniformity (the extensional contribution). It exists only when the flow is oblique to the surface, $\vec{u}_o \times \vec{n} \neq 0$. The contraction or expansion of the flame surface depends on the sign of the surface divergent of the tangent component of the flame velocity. In the second term, $\vec{v}_F \cdot \vec{n} = S_F = \vec{u}_o \cdot \vec{n} + S_d$ is the normal velocity of the flame surface. The second term, $(\vec{v}_F \cdot \vec{n})(\nabla \cdot \vec{n}) = S_F\ (\nabla \cdot \vec{n})$, is the stretch rate caused by flame unsteadiness and curvature of the flame surface (the dilatational contribution). This term can be divided in the normal strain rate, $(\vec{u}_o \cdot \vec{n})\,(\nabla \cdot \vec{n})$, and the displacement speed, $S_d\,(\nabla \cdot \vec{n})$, effects. The curvature, $\kappa = \nabla \cdot \vec{n}$, is positive when the flame is convex towards the unburned gas. The tip of a bunsen burner is concave towards the unburned mixture, therefore presenting negative curvature.

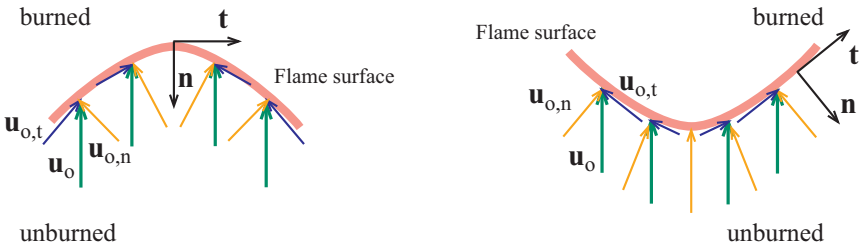

(a) Concave towards the unburned mixture:
$\kappa = \nabla \cdot \vec{n} < 0$
$\nabla_t \cdot \vec{u}_{o,t} < 0$
$(\vec{u}_o \cdot \vec{n})\ \kappa > 0$
$S_d(\nabla \cdot \vec{n}) < 0$

(b) Convex towards the unburned mixture:
$\kappa = \nabla \cdot \vec{n} > 0$
$\nabla_t \cdot \vec{u}_{o,t} > 0$
$(\vec{u}_o \cdot \vec{n})\ \kappa < 0$
$S_d(\nabla \cdot \vec{n}) > 0$

Figure 2: Effect of flame curvature on stretch rate. The green arrows are the flow field at the flame surface $\vec{u}_o$, assumed uniform, the yellow vectors are the normal component $\vec{u}_{o,n}$ and the blue vectors are the tangent component $\vec{u}_{o,t}$.

Figure 2 illustrates the effect of flame curvature on stretch rate. A uniform flow velocity field $\vec{u}_o$ is used for simplicity. Figure 2a presents a flame surface that is concave towards the unburned mixture. The tangent component of the flow velocity $\vec{u}_{o,t}$ points towards the vertex, thus resulting in flame compression. This effect is expressed by the tangential strain rate component. The tangent component of the flow velocity at the surface $\vec{u}_{o,t}$ decreases towards the vertex. Therefore, the tangential strain rate is negative, $\nabla_t \cdot \vec{u}_{o,t} < 0$, indicating flame compression. The normal strain rate depends on the normal component of the flow velocity and flame curvature. The normal component of the flow velocity at the surface $\vec{u}_{o,n}$ is negative and the curvature is also negative, $\kappa = \nabla \cdot \vec{n} < 0$. Then, the normal strain rate becomes positive, $(\vec{u}_o \cdot \vec{n})\ \kappa > 0$. For the convex surface, Fig. 2b, the tangential component of the flow velocity results in flame extension, which is confirmed by $\nabla_t \cdot \vec{u}_{o,t} > 0$. For the normal strain rate, the curvature is positive, $\kappa = \nabla \cdot \vec{n} > 0$, and $(\vec{u}_o \cdot \vec{n})\ \kappa < 0$.

For a stationary flame, $\vec{v}_F = 0$ and the second term of Eq. (10) is identically equal to zero. The tangential component of the flame surface velocity, in the flame sheet approximation, is equal to the tangential component of the flow velocity at the flame surface, $\vec{v}_{F,t} = \vec{u}_{o,t}$, while $\vec{v}_{F,n} = \vec{u}_{o,n} + S_d\,\vec{n} = 0$. Therefore,

$$\mathrm{K} = \nabla_t \cdot \vec{v}_{F,t} = \nabla_t \cdot \vec{u}_{o,t} = \nabla_t \cdot (\vec{u}_o - \vec{u}_{o,n}) = \nabla_t \cdot \vec{u}_o + S_d\,\nabla \cdot \vec{n}. \tag{11}$$

As a result, for the stationary flame, the concave surface of Figure 2a experiences compression and the stretch rate is negative, $\mathrm{K} < 0$, while that for Figure 2b experiences extension and the stretch rate is positive, $\mathrm{K} > 0$. Using the definition of Karlovitz number, $\mathrm{Ka} = \mathrm{K}(\delta_l^0/S_l^0)$, Eq. (11) may be nondimensionalized as

$$\mathrm{Ka} = \mathrm{Ka_s} + \mathrm{Ka_c}, \tag{12}$$

where the tangential strain and curvature effects are

$$\mathrm{Ka_s} = \frac{\delta_l^0}{S_l^0}\nabla_t \cdot \vec{u}_o, \qquad \mathrm{Ka_c} = \frac{\delta_l^0}{S_l^0} S_d\,\nabla \cdot \vec{n}. \tag{13}$$

This definition of stretch rate may be used in the G-equation formulation and a better approximation for the displacement velocity S_d can be obtained with the thin flame model, as follows.

3.1 Thin flame approximation

The next level of amplification, reveals the flame preheating zone, with characteristic length scale δ_l, and a thin reaction zone, with characteristic length scale $\delta_r \ll \delta_l$. They are identified in Fig. 1.

The flame surface can be associated to the iso-surface of a flame scalar property. One possibility is to take an iso-concentration line of a reactant i as the locus of the flame surface. Then, the flame surface is the iso-surface $Y_i(\vec{x}, t) = Y_{i,0}$, where $Y_{i,0}$ is a constant that will be defined later. Considering that Y_i is consumed in the flame, the surface unit normal vector becomes

$$\vec{n} = \frac{\nabla Y_i}{|\nabla Y_i|}. \tag{14}$$

The flame is a surface of constant mass fraction that is Lagrangian advected by $\vec{v}_F$. Therefore, on the flame surface,

$$\frac{dY_i}{dt} = \frac{\partial Y_i}{\partial t} + \vec{v}_F \cdot \nabla Y_i = 0. \tag{15}$$

The conservation equation for the species i, may be written as

$$\rho\frac{\partial Y_i}{\partial t} + \rho\vec{u}\cdot\nabla Y_i = \nabla\cdot(\rho D_{i,m}\nabla Y_i) + \dot{\omega}_i, \tag{16}$$

where $D_{i,m}$ is a diffusion coefficient of species i in the mixture and $\dot{\omega}_i$ is the species production/consumption by chemical reaction. Applying this equation on the flame surface, using Eq. (15) for the transient term, and recalling that $\vec{v}_F = \vec{u}_o + S_d\,\vec{n}$,

$$S_d = -\frac{\nabla\cdot(\rho D_{i,m}\nabla Y_i) + \dot{\omega}_i}{\rho|\nabla Y_i|}, \tag{17}$$

where all operations are taken on the flame surface. From Eq. (14), the divergent term in the right-hand side may be expanded as,

$$\nabla\cdot(\rho D_{i,m}\nabla Y_i) = \rho D_{i,m}|\nabla Y_i|\,(\nabla\cdot\vec{n}) + \vec{n}\cdot\nabla\left(\rho D_{i,m}\,\vec{n}\cdot\nabla Y_i\right). \tag{18}$$

The first term in the right-hand side accounts for the flame curvature, $\kappa = \nabla\cdot\vec{n}$. The second term is the contribution of the normal diffusion to the displacement speed. Naming this contribution S_n and naming the reaction contribution S_r, the displacement speed from Eq. (17) becomes

$$S_d = -D_{i,m}\kappa - S_n - S_r, \tag{19}$$

where,

$$\rho|\nabla Y_i|S_n = \vec{n}\cdot\nabla\left(\rho D_{i,m}\,\vec{n}\cdot\nabla Y_i\right), \qquad \rho|\nabla Y_i|S_r = \dot{\omega}_i. \tag{20}$$

For an unstretched, planar, steady flame, $S_n + S_r = -S_l^0$. For the thin flame, however, the curvature, gradient of mass fraction and reaction affect the flame displacement speed.

The iso-surface representing the flame surface used for calculating S_d is typically selected within the flame, where variations in density from its unburned value ρ_u have taken place, affecting the mass flux through this surface. For a meaningful comparison between values of the displacement speed defined at different locations, S_d is often normalized by the ratio of local density ρ to the density if the fresh mixture ρ_u yielding,

$$\tilde{S_d} = \frac{\rho S_d}{\rho_u}. \tag{21}$$

The density-weighted flame displacement speed, $\tilde{S_d}$, can be directly compared to the laminar flame speed S_l^0 for the same reactant mixture.

An order of magnitude estimate can be derived applying Eq. (19) to the flame structure represented in Fig. 1. Using $\nabla = (\partial/\partial n)\,\vec{n} + (\partial/\partial t)\,\vec{t}$, where t is the tangent direction, we have

$$S_d = -D_{i,m}\kappa - \frac{1}{\rho\left[(\partial Y_i/\partial n)^2 + (\partial Y_i/\partial t)^2\right]^{1/2}}\left[\frac{\partial}{\partial n}\left(\rho D_{i,m}\frac{\partial Y_i}{\partial n}\right) + \dot{\omega}_i\right]. \tag{22}$$

Noting that the term within brackets is equal to $(-\rho_u S_u \partial Y_i/\partial n)$, neglecting the variation of Y_i in the tangent direction, and using $D_{i,m} = D_T/\mathrm{Le}$,

$$S_d \simeq -\frac{D_T\kappa}{\mathrm{Le}} + \frac{\rho_u S_u}{\rho}. \tag{23}$$

Therefore, the nondimensional density-weighted flame displacement speed becomes

$$\frac{\tilde{S_d}}{S_l^o} \simeq \frac{S_u}{S_l^o} - \frac{\rho D_T\kappa}{\rho_u S_l^o \mathrm{Le}}. \tag{24}$$

This expression evidences the effect of flame curvature and Lewis number in the displacement speed. The flame displacement becomes greater than the laminar flame speed, $\tilde{S_d} > S_u$, when the curvature is negative, $\kappa < 0$. Also, the density-weighted flame displacement speed increases as the Lewis number becomes larger than one, when $\mathrm{Le} > 1$. At the tip of the Bunsen flame, the curvature is negative and $\tilde{S_d} > S_u$. We can also notice that extinction is bound to occur when $\kappa \geq \rho_u S_u \mathrm{Le}/\rho D_T$. A fuel with larger Lewis number is more resistant to extinction by flame stretch.

The description above forms the classical understanding of the effects of flame stretch rate in the displacement flame speed. From the measurement point of view, several authors have invested a considerable effort in devising ways to reduce heat loss and in correctly accounting for the effect of flame stretch rate in laboratory flames, such that the local consumption speed approximates adequately the laminar flame speed, i.e., the speed of a planar, adiabatic flame (Egolfopoulos *et al.*, 2014). Two aspects are not taken into account in the thin flame approach reviewed above: (1) The transport of heat and mass is restricted to the normal direction. Tangential transport is not accounted for. The temperature and mass fraction gradients are smaller in the tangential direction, however, as flames become weaker, their thermal thickness increase and flame stability becomes affected by transport along the flame. (2) Variable transport properties and detailed chemistry are not taken into account. Therefore, the effects of phenomena, such as cool flame, cannot be analyzed. Cool flames occur for fuels exhibiting negative temperature coefficient (NTC) ignition delay time curves at unburned temperatures from 600 K to 900 K at normal and high pressures (Battin-Leclerc, 2008), (Goldsborough *et al.*, 2017).

To account for these effects, a full DNS model is needed. Here, the results of a DNS model are used to calculate the displacement speed using the classical formulation of the thin flame model given by Eq. (19).

4. COMPUTATIONAL METHODS

The simulations were performed using the direct numerical simulation code EBI-DNS (Engler-Bunte-Institut), which solves the governing equations employing the finite volume method (Zirwes *et al.*, 2020). The fully compressible Navier-Stokes, species and energy equations for reacting gas mixtures are solved coupled to the chemical kinetics library Cantera (Goodwin, 2002). Cantera's treatment of chemical reactions was implemented utilizing OpenFOAM's (OpenCFD, 2011) standard capabilities of modeling non-reactive flows. The pressure-implicit split-operator (PISO) algorithm has been used for the pressure correction (Ferziger and Peric, 2002).

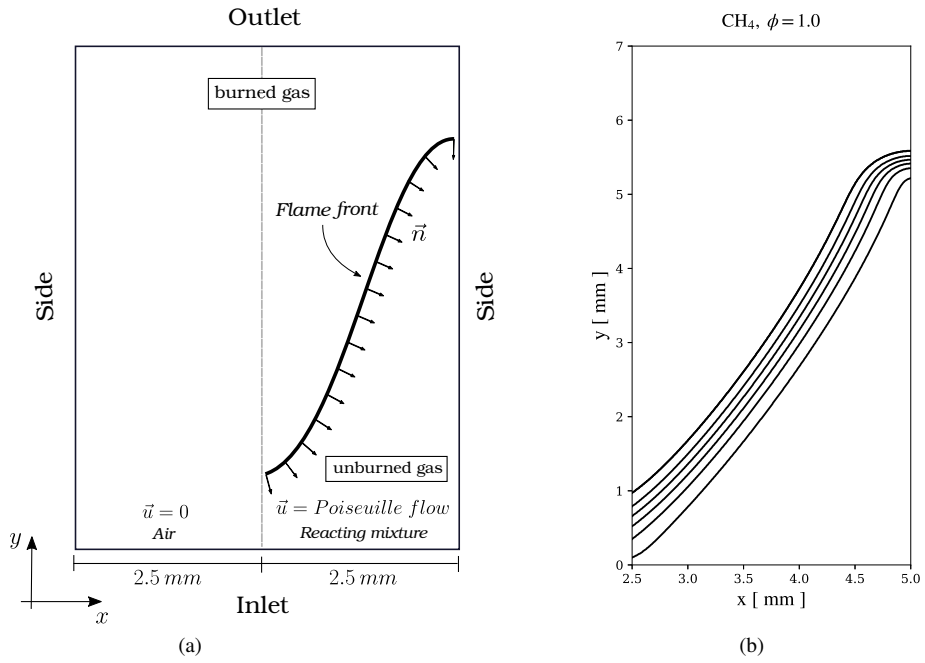

Figure 3: (a) Computational domain and (b) Isotherm lines from 400 K to 1900 K, at 300 K temperature steps, for the methane/air flame at $\phi = 1$.

Figure 3a presents the computational domain. The simulation was carried out in a two-dimensional rectangular domain with a height of 20 mm in the stream-wise direction and 10 mm of width. The slot outlet has a width of 10 mm. A Poiseuille velocity profile is imposed in the slot outlet and zero velocity is enforced in the remaining of the bottom face. The partially non-reflecting boundary condition has been applied to the inlet and outlet boundaries for pressure, to bypass sound waves at those boundaries. The unburned gas temperature T_u is prescribed at the burner rim. At the sides of the domain, a zero gradient condition was enforced (Rastigejev and Matalon, 2006). The computational domain uses a rectangular structured mesh with, at least, 30 cells to resolve the flame thickness.

Methane/air (CH_4) and dimethyl-ether/air (CH_3OCH_3) premixed flames are solved at two equivalence ratios, $\phi = 0.7$ and $\phi = 1$, at $T_u = 298K$ and atmospheric pressure. For the methane/air simulations, the reduced mechanism of Kee *et al.* (1985) with 17 species and 58 elementary reactions was used. The simulations for dimethyl-ether/air mixtures used a reduced chemical mechanism consisting of 30 species and 175 reactions, with 9 species assumed to exist under

quasi-steady state (Bhagatwala *et al.*, 2015).

In the following analysis, two definitions of the flame surface position are used according to the laminar, planar, adiabatic flame solved by Cantera. The first places the flame surface in the preheating zone by setting $Y_{f,o} = 0.9\ Y^o_{f,u}$. The second choice places the flame within the reaction zone by defining the flame as the mass fraction iso-line where the maximum heat release rate occurs (Zhang *et al.*, 2016). This is represented as $Y_{f,o} = Y^o_f(\dot{q}_{max})$. Table 1 presents the laminar, planar, adiabatic flame parameters for the methane/air and dimethyl-ether/air flames solved here ($T_u = 298$ K, $p = 100$ kPa). In Tab. 1, $Y_{f,o}(0.9\ Y_{f,u})$ and $Y_{f,o}(\dot{q}_{max})$ are the values of the iso-lines of mass fraction for the two definitions of flame surface positions, $\langle u \rangle_{inlet}$ is the reactant mixture mean axial velocity at the inlet boundary condition and Le_{eff} is the effective Lewis number. This represents the average value of the fuel and oxidizer Lewis numbers weighted more heavily with respect to the deficient component in the mixture, (Matalon *et al.*, 2003).

Table 1: Laminar, planar, adiabatic flame parameters for the methane/air and dimethyl-ether/air flames solved here ($T_u = 298$ K, $p = 100$ kPa).

Fuel	ϕ	S^0_l, cm/s	δ^0_l, mm	T_b, K	Le_{eff}	$\langle u \rangle_{inlet}$, cm/s	$Y_{f,o}(0.9\ Y_{f,u})$	$Y_{f,o}(\dot{q}_{max})$
CH_4	1.0	37.0	0.46	2230	1.00	80.0	0.0495	0.0033
CH_4	0.7	19.0	0.66	1844	0.95	35.0	0.0351	0.0024
DME	1.0	47.0	0.26	2290	1.23	80.0	0.0900	0.0019
DME	0.7	26.0	0.44	1934	1.43	45.0	0.0648	0.0009

5. RESULTS AND ANALYSIS

Figure 3b presents the isotherm lines from 400 K to 1900 K for the methane/air flame at $\phi = 1$. The flame is anchored at the burner rim and the liftoff distance is under 1 mm. The deformation caused by the flow field on the flame surface is visible. At the flame tip, the temperature iso-lines are closer, while near to the burner rim, the opposite occurs. The flame has a more flat profile in the intermediate region between the base and the tip.

Figure 4 shows the field of rate of production of fuel for the 4 cases run. DME at $\phi = 1$, Fig. 4c, presents the higher laminar flame speed (see Tab. 1), resulting in a thinner flame, shorter cone and smaller liftoff distance. As the equivalence ratio is reduced to $\phi = 0.7$, the flame thickness and liftoff distance increase, more significantly for methane, than for DME. The flame tail is also displaced to a position farther from the slot half width, resulting in fuel leakage and air entertainment.

The fuel heat release increases towards the tip for both fuels, mainly as a response to the Poiseuille flow profile at the slot exit. DME/air mixtures have a Lewis number above unity (see Tab. 1), meaning that heat transfer penetrates further than fuel mass transfer. Therefore, there is a focusing effect of heat in the tip of the burner, leading to preheating of the unburned mixture, increasing the reaction rate further. Methane/air mixtures have a Lewis number equal or slightly under unity, meaning that the mass and heat transfer stay in balance.

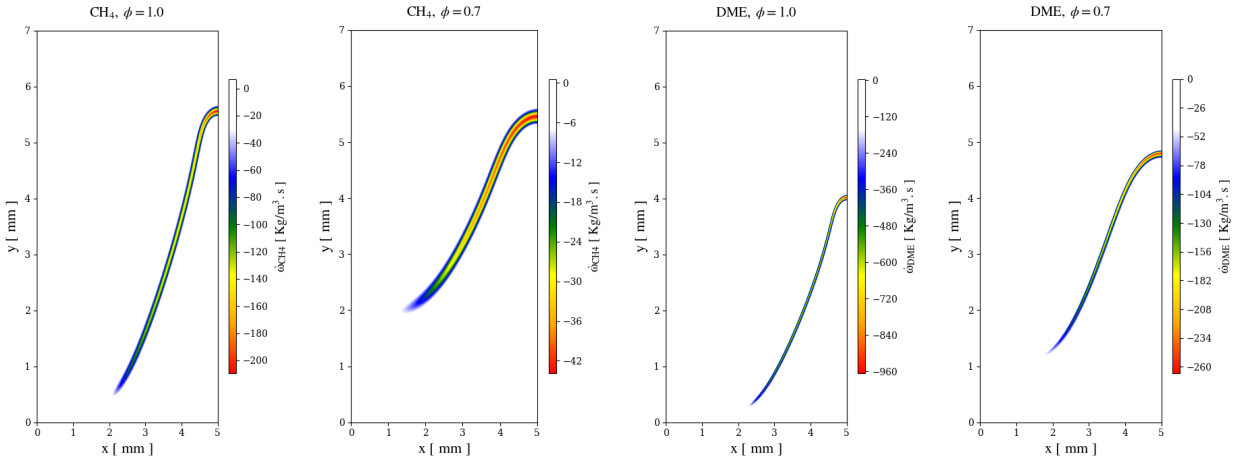

Figure 4: Fuel reaction rate, (a) methane, $\phi = 1.0$, (b) methane, $\phi = 0.7$, (c) DME, $\phi = 1.0$, and (d) DME, $\phi = 0.7$.

The results calculated from the application of Eq. (10) are presented in Fig. 5, plotted as Karlovitz number as a function of the dimensionless flame length. The dimensionless flame length is taken along the selected iso-line. Figure

5a presents the strain $\mathrm{Ka_s}$ and curvature $\mathrm{Ka_c}$ contributions for the stretch rate, as defined in Eq. (12), for the iso-line at $Y_{f,o}(\dot{q}_{max})$. The strain and curvature effects are both positive and equivalent up to $s/s_{max} = 0.75$. Near the tip, the strain effect becomes positive and the curvature negative, as anticipated. The sum of both effects is a negative stretch rate. The $Y_{f,o}(0.9\,Y_{f,u})$ presents a similar behavior except that the curvature effect is near zero for $s/s_{max} < 0.9$. Since the strain rate effect is positive, the overall stretch rate is positive up to $s/s_{max} = 0.9$ and then becomes negative, as anticipated, but with a sharper slope. From Fig. 5a and 5b, we note that the $Y_{f,o}(\dot{q}_{max})$ definition is more sensitive to variations in flame curvature, and, therefore, will be used for the remaining analysis.

Figures 5c and 5d compare the overall Karlovitz number of methane and DME flames for $Y_{f,o}(\dot{q}_{max})$, for both equivalence ratios. The flames for $\phi = 0.7$ present a more non-uniform Karlovitz number profile, indicating that this condition is more affected by curvature, since the fuel reaction rate is weaker, as anticipated in Eq. (8). The nondimensional stretch rate is positive up to s/s_{max} between 0.65 and 0.7.

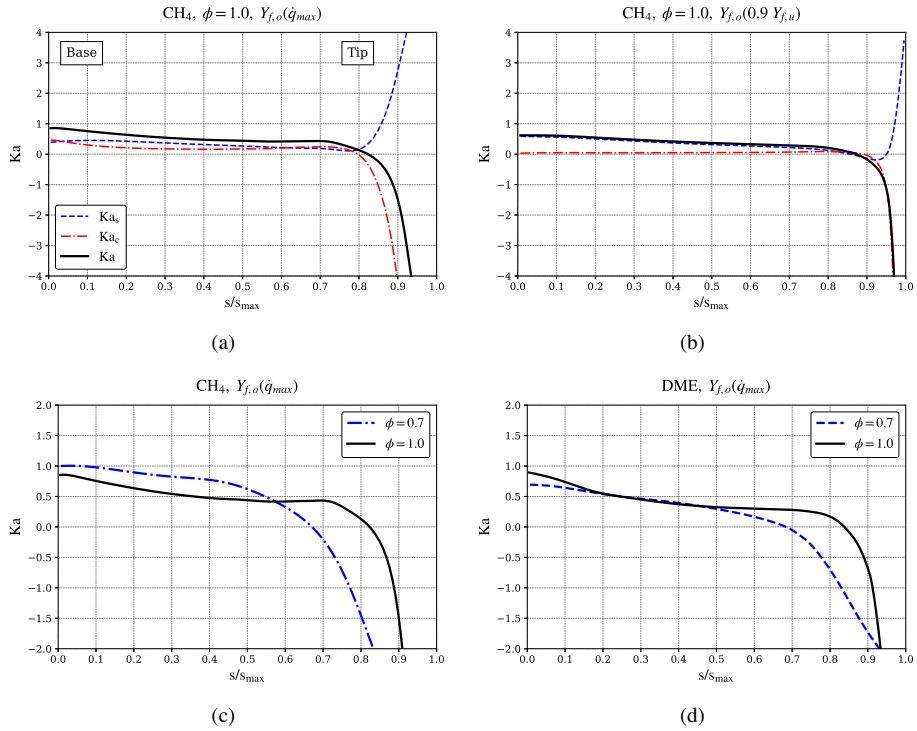

Figure 5: Karlovitz number as function of non-dimensional flame length, (a) Strain $\mathrm{Ka_s}$ and curvature $\mathrm{Ka_c}$ effects and overall Karlovitz number Ka for $\mathrm{CH_4}$, $\phi = 1$, and $Y_{f,o}(\dot{q}_{max})$, (b) Strain $\mathrm{Ka_s}$ and curvature $\mathrm{Ka_c}$ effects and overall Karlovitz number Ka for $\mathrm{CH_4}$, $\phi = 1$, and $Y_{f,o}(0.9\,Y_{f,u})$, (c) Overall Karlovitz number Ka for $\mathrm{CH_4}$, $\phi = 1$ and $\phi = 0.7$, (d) Overall Karlovitz number Ka for DME, $\phi = 1$ and $\phi = 0.7$.

Figure 6 shows the nondimensional normalized displacement speed $\tilde{S}_d/S_l^o$ for the $Y_{f,o}(\dot{q}_{max})$ for both fuels, at both equivalence ratios. Both fuels present the same general trends, indicating that the curvature term prevails in Eq. (19). The stoichiometric flames present steeper gradients and a larger variation than the lean flames. The flames for both fuels change from $\tilde{S}_d/S_l^o$ lower to one to higher to one at the same nondimensional flame surface coordinate. Near the tip, the methane flame presents a larger positive deviation from the laminar planar flame speed, as a result of the larger curvature.

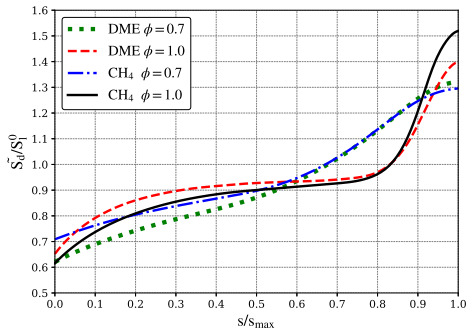

Figure 6: Nondimensional normalized displacement speed as a function of the nondimensional flame arc-length.

In Fig. 7 is shown the correlation of nondimensional normalized displacement speed to Karlovitz number. The general trends are: Near the base, the Karlovitz number tends to one and the displacement speed is smaller than the laminar flame speed as a result of positive curvature and heat loss to the burner rim. Towards the tip, the Karlovitz number becomes negative due to negative curvature and the displacement flame speed increases in respect to the laminar flame speed. The stoichiometric flames present sharper tip and therefore reach larger values of Karlovitz number.

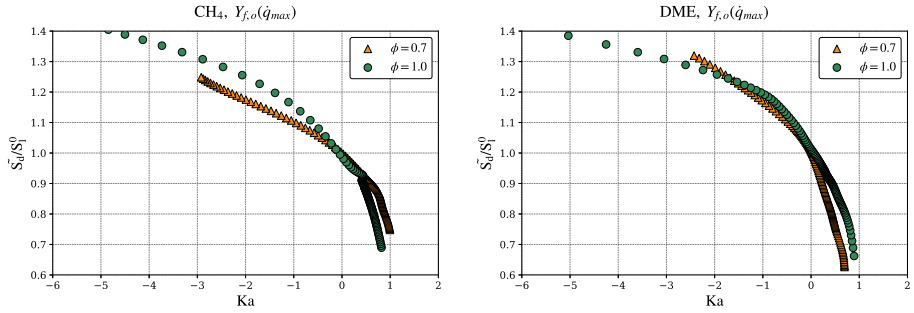

(a) (b)

Figure 7: Correlation between nondimensional normalized weighted displacement speed and Karlovitz number.

The structure of the two-dimensional flame is affected by tangent components of convection and diffusion fluxes, disturbing the local mass fraction distributions. Figure 8 presents the relative, two-dimensional, species i mass fraction along the flame surface, $\hat{Y}_i^0 = Y_i/Y_i^0$, where Y_i^o is the value calculated for the planar, adiabatic flame. The figure presents the curves for hydrogen and oxygen for the two choices of flame surface position. For methane at $\phi = 1$, the concentration of oxygen has a negligible variation ($D_{m,\mathrm{H_2}} > D_{m,\mathrm{CH_4}} > D_{m,\mathrm{O_2}}$). Due to its higher difffusivity, hydrogen, on the other hand, presents a larger variation. Hydrogen is formed at the reaction region and diffuses to the unburned mixture. Therefore, the regions with positive curvature (near the base) present deficiency and regions with negative curvature (near the tip) present excess hydrogen. The stoichiometric flame presents higher curvature near the tip (Fig. 8a), therefore, higher excess when compared to the lean flame (Fig. 8b). The lean flame, however, presents a higher positive curvature near the base and therefore, the deficiency of hydrogen is larger. When the flame surface is chosen within the reaction region, the hydrogen profile is deficient in most of the flame surface, as a result of the diffusion to the unburned region. DME has the lower diffusion coefficient ($D_{m,\mathrm{H_2}} > D_{m,\mathrm{O_2}} > D_{m,\mathrm{DME}}$). Oxygen diffuses from the unburned mixture to the reaction region. Therefore, oxygen becomes deficient along the flame and the effect increases as curvature increases (Fig. 8c and 8d).

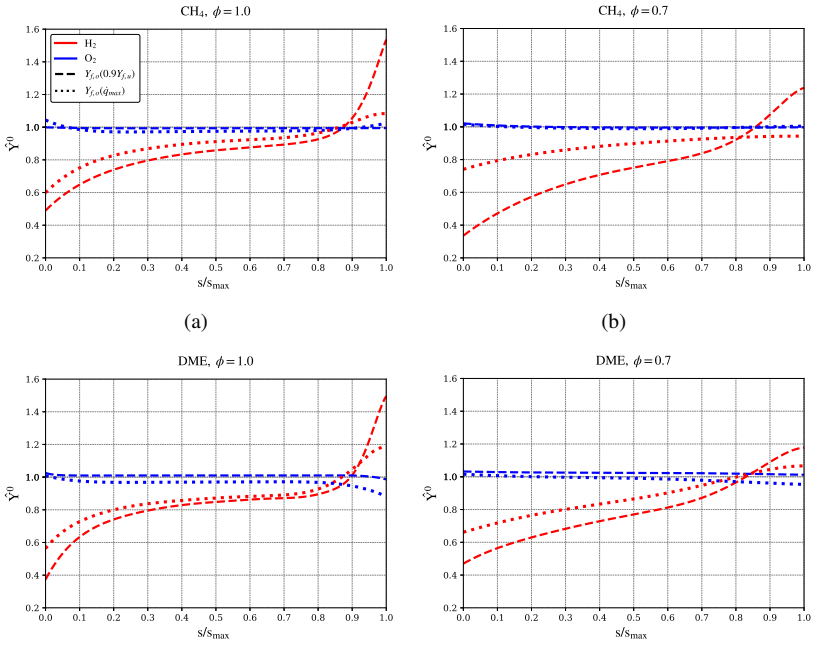

(a) (b)

(c) (d)

Figure 8: Relative, two-dimensional mass fractions of hydrogen and oxygen along the flame surface, $\hat{Y}_i^0 = Y_i/Y_i^0$, where Y_i^o is the value calculated for the planar, adiabatic flame.

Figures 9 and 10, in the first row, present the normal distributions of temperature, hydrogen and oxygen mass fractions for the methane flame at $\phi = 1$. Figures 9 and 10, in the second row, show the normal distributions of the hydrogen and oxygen reaction rates (d and e) and the heat release and volumetric energy diffusion (f). Figure 10 present the same results for the methane flame at $\phi = 0.7$. The curves correspond to two positions along the flame surface, one around half the flame height, where $\tilde{S}_d/S_l^0 = 0.83$, and the other near the tip, where $\tilde{S}_d/S_l^0 = 1.45$. The dotted line is the result for the planar, adiabatic flame for the same positions. The triangular markers identify the position of the flame surface for $Y_{f,o}(0.9\, Y_{f,u})$.

The hydrogen distribution for the positively curved region (in red, Fig. 9a) presents a deficiency in the preheating and post-reaction region. Both the production and destruction rates in Fig. 9d are reduced. The oxygen mass fraction is not strongly affected (Fig. 9b), but the hydrogen deficiency has an effect in the oxygen destruction rate (Fig. 9e). As a result, both the energy diffusion flux and heat release are reduced (Fig. 9f). The distributions for the region with negative curvature (in green) follow the opposite trend. The temperature distribution (Fig. 9c) shows that in the region with positive curvature (in red) the equilibrium temperature is smaller than the temperature of the planar, adiabatic flame. The region with negative curvature (in green) shows the opposite trend, in which the temperature gradient is greater than the planar, adiabatic flame. The results for the lean flame in Fig. 10 present the same trends, but with smaller intensity.

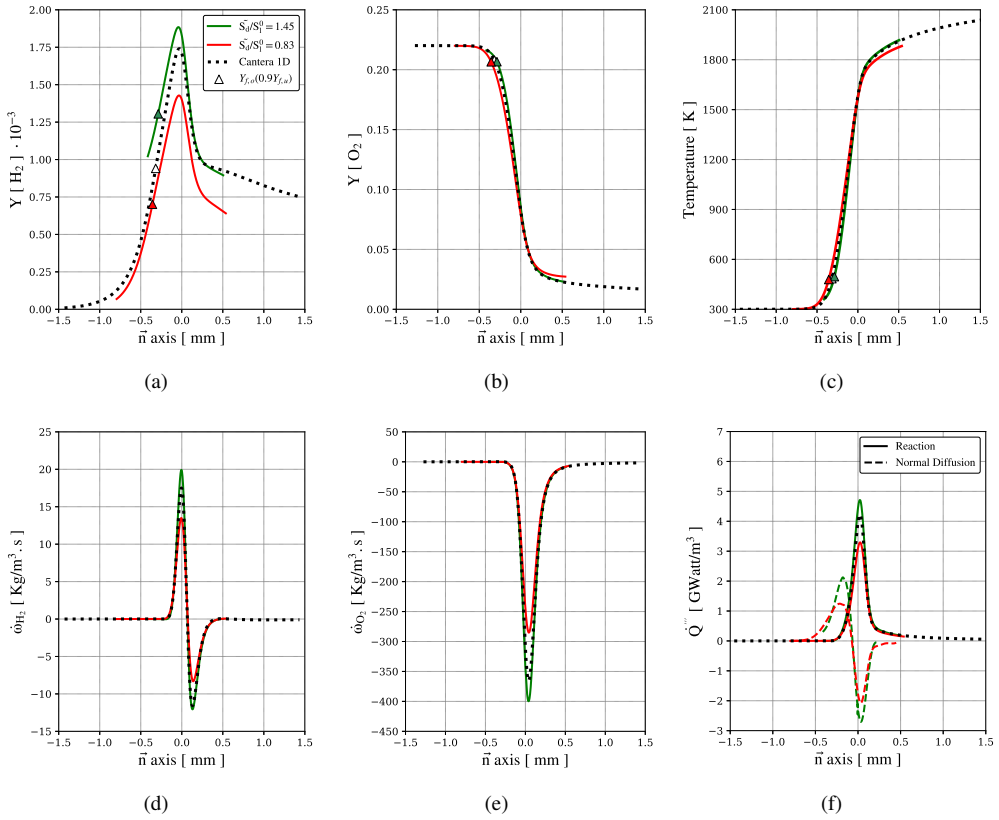

Figure 9: Normal flame distributions for the methane flame, at $\phi = 1$, for two positions along the flame surface, one around half the flame height, where $\tilde{S}_d/S_l^0 < 1$, and the other near the tip, where $\tilde{S}_d/S_l^0 > 1$. The dotted line is the result for the planar, adiabatic flame for the same positions. The triangular markers identify the position of the flame surface for $Y_{f,o}(0.9\, Y_{f,u})$. (a) hydrogen mass fraction, (b) oxygen mass fraction, (c) temperature, (d) hydrogen reaction rate, (e) oxygen reaction rate and (f) heat release rate and volumetric energy diffusion.

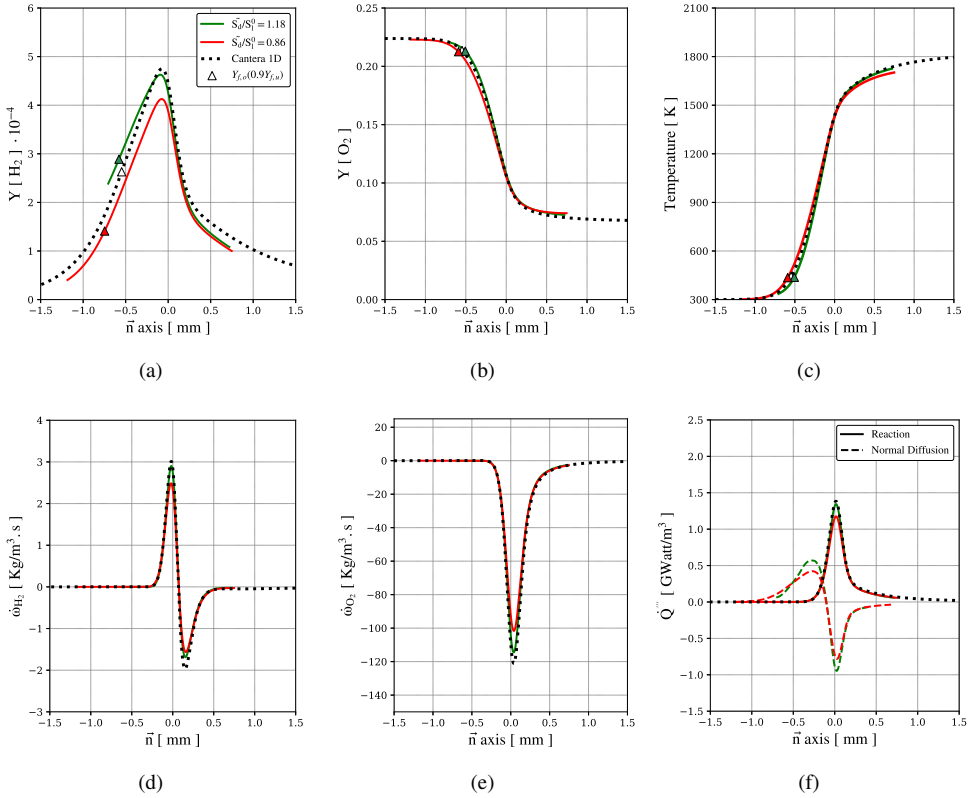

Figure 10: Normal flame distributions for the methane flame, at $\phi = 0.7$, for two positions along the flame surface, one around half the flame height, where $\tilde{S}_d/S_l^0 < 1$, and the other near the tip, where $\tilde{S}_d/S_l^0 > 1$. The dotted line is the result for the planar, adiabatic flame for the same positions. The triangular markers identify the position of the flame surface for $Y_{f,o}(0.9\ Y_{f,u})$. (a) hydrogen mass fraction, (b) oxygen mass fraction, (c) temperature, (d) hydrogen reaction rate, (e) oxygen reaction rate and (f) heat release rate and volumetric energy diffusion.

6. SUMMARY AND OUTLOOKS

The effects of flame curvature, normal and tangential strains in the flame stretch rate and flame displacement speed are studied using DNS for slot burner flames of two fuels: methane and DME, at $\phi = 1$ and $\phi = 0.7$. Methane flame presents fuel Lewis number near one and DME flame presents fuel Lewis number above one. The slot flame presents positive curvature near the base and negative curvature near the tip.

The strain and curvature contributions to the Karlovitz number have the same intensity in the region of positive curvature, but the curvature contribution becomes strongly negative and dominant in the concave curvature region. The stoichiometric flames present stronger variations of Karlovitz number when compared to the lean flames. The dimensionless displacement speed normalized by the laminar flame speed (planar flame) is smaller than one in the region of positive curvature and grows above one in the region of negative curvature. The correlation with Karlovitz number is similar for both fuels and stoichiometries.

The mass fraction of hydrogen along the flame surface presents strong deficiency in the positive curvature region and strong excess in the negative curvature region when compared to the planar, adiabatic flame. The trend is observed not only on the position of the flame surface, but also in the entire distribution along the normal direction as well.

The next steps in this research are the extension for more complex fuels, for which cool flame is observed, and the application of this numerical model for transient flames, in order to observe the contribution of flame unsteadiness in the flame stretch and displacement speed.

7. ACKNOWLEDGMENTS

The authors gratefully acknowledge the research group of Engler-Bunte-Institute, Division of Combustion Technology, Karlsruhe Institute of Technology, Germany, for providing the EBI-DNS solver, the support of the Scientific Computation Laboratory of Campus Joinville/UFSC, of the Graduate Program in Mechanical Engineering at Federal University of Santa Catarina, Brazil, and the National Council for Scientific and Technological Development, Brazil, for the scholarship of the leading author.

8. REFERENCES

Battin-Leclerc, F., 2008. "Detailed chemical kinetic models for the low-temperature combustion of hydrocarbons with application to gasoline and diesel fuel surrogates". *Progress in Energy and Combustion Science*, Vol. 34, No. 4, pp. 440 – 498.

Bhagatwala, A., Luo, Z., Shen, H., Sutton, J., Lu, T. and Chen, J., 2015. "Numerical and experimental investigation of turbulent dme jet flames". *Proceedings of the Combustion Institute*, Vol. 35, No. 2, pp. 1157–1166.

Egolfopoulos, F., Hansen, N., Ju, Y., Kohse-Höinghaus, K., Law, C. and Qi, F., 2014. "Advances and challenges in laminar flame experiments and implications for combustion chemistry". *Progress in Energy and Combustion Science*, Vol. 43, pp. 36 – 67.

Ferziger, J.H. and Peric, M., 2002. *Computational Methods for Fluid Dynamics*. Springer, Berlin.

Goldsborough, S.S., Hochgreb, S., Vanhove, G., Wooldridge, M.S., Curran, H.J. and Sung, C.J., 2017. "Advances in rapid compression machine studies of low- and intermediate-temperature autoignition phenomena". *Progress in Energy and Combustion Science*, Vol. 63, pp. 1 – 78.

Goodwin, D.G., 2002. *Cantera C++ user's guide*. California Institute of Technology, California.

Kee, R., Grcar, J., Smooke, M., Miller, J. and Meeks, E., 1985. "Premix: A fortran program for modeling steady laminar one-dimensional premixed flames". *Sandia National Laboratories*.

Law, C.K., 2006. *Combustion Physics*. Cambridge University Press, Cambridge.

Matalon, M., Cui, C. and Bechtold, J., 2003. "Hydrodynamic theory of premixed flames: Effects of stoichiometry, variable transport coefficients and arbitrary reaction orders". *Journal of Fluid Mechanics*, Vol. 487, pp. 179 – 210.

OpenCFD, 2011. "Openfoam user guide". version 2.0.1.

Peters, N., 2000. *Turbulent Combustion*. Cambridge University Press, New York.

Poinsot, T. and Veynante, D., 2005. *Theorical and Numerical Combustion*. Edwards, Philadelphia, 2nd edition.

Rastigejev, Y. and Matalon, M., 2006. "Numerical simulation of flames as gas-dynamic discontinuities". *Combustion Theory and Modelling*, Vol. 10, No. 3, pp. 459–481.

Selle, L., Poinsot, T. and Ferret, B., 2011. "Experimental and numerical study of the accuracy of flame-speed measurements for methane/air combustion in a slot burner". *Combustion and Flame*, Vol. 158, No. 1, pp. 146 – 154.

Zhang, F., Zirwes, T., Habisreuther, P. and Bockhorn, H., 2016. "Effect of unsteady stretching on the flame local dynamics". *Combustion and Flame*, Vol. 175, pp. 170 – 179.

Zirwes, T., Zhang, F., Habisreuther, P., Hansinger, M., Bockhorn, H., Pfitzner, M. and Trimisn, D., 2020. "Quasi-dns dataset of a piloted flame with inhomogeneous inlet conditions". *Flow, Turbulence and Combustion*, Vol. 104, pp. 997–1027.

9. RESPONSIBILITY NOTICE

The authors are solely responsible for the printed material included in this paper.